

Article

# Evaluating Carbon Sequestration and PM<sub>2.5</sub> Removal of Urban Street Trees Using Mobile Laser Scanning Data

Yingyi Zhao <sup>1</sup>, Qingwu Hu <sup>1,2,\*</sup> , Haidong Li <sup>2,3</sup> , Shaohua Wang <sup>1</sup> and Mingyao Ai <sup>1</sup>

<sup>1</sup> School of Remote Sensing and Information Engineering, Wuhan University, Wuhan 430079, China; zhaoyingyi@whu.edu.cn (Y.Z.); shwang@whu.edu.cn (S.W.); aimingyao@whu.edu.cn (M.A.)

<sup>2</sup> Nanjing Institute of Environmental Sciences, Ministry of Environmental Protection, Nanjing 210042, China; lihd2020@163.com

<sup>3</sup> Key Laboratory for National Geography State Monitoring (National Administration of Surveying, Mapping and Geoinformation), Wuhan University, Wuhan 430079, China

\* Correspondence: huqw@whu.edu.cn; Tel.: +86-189-7107-0362

Received: 28 September 2018; Accepted: 4 November 2018; Published: 7 November 2018



**Abstract:** Street trees are an important part of urban facilities, and they can provide both aesthetic benefits and ecological benefits for urban environments. Ecological benefits of street trees now are attracting more attention because of environmental deterioration in cities. Conventional methods of evaluating ecological benefits require a lot of labor and time, and establishing an efficient and effective evaluating method is challenging. In this study, we investigated the feasibility to use mobile laser scanning (MLS) data to evaluate carbon sequestration and fine particulate matter (PM<sub>2.5</sub>) removal of street trees. We explored the approach to extract individual street trees from MLS data, and street trees of three streets in Nantong City were extracted. The correctness rates and completeness rates of extraction results were both over 92%. Morphological parameters, including tree height, crown width, and diameter at breast height (DBH), were measured for extracted street trees, and parameters derived from MLS data were in a good agreement with field-measured parameters. Necessary information about street trees, including tree height, DBH, and tree species, meteorological data and PM<sub>2.5</sub> deposition velocities were imported into i-Tree Eco model to estimate carbon sequestration and PM<sub>2.5</sub> removal. The estimation results indicated that ecological benefits generated by different tree species were considerably varied and the differences for trees of the same species were mainly caused by the differences in morphological parameters (tree height and DBH). This study succeeds in estimating the amount of carbon sequestration and PM<sub>2.5</sub> removal of individual street trees with MLS data, and provides researchers with a novel and efficient way to investigate ecological benefits of urban street trees or urban forests.

**Keywords:** ecological benefits; i-Tree Eco model; LiDAR; MLS; morphological parameters; street trees extraction

## 1. Introduction

Rapid urbanization tends to increase urban temperature, carbon dioxide (CO<sub>2</sub>) emission, and ozone levels, which make urban areas warmer than rural areas [1]. CO<sub>2</sub> is the dominant greenhouse gas [2]. Fuel combustion, air pollution, decreasing urban green land, and some other factors lead to higher temperatures and more CO<sub>2</sub> in cities. Urban forests play an essential role in urban environment and street trees are an important part of urban forests [3]. Trees can fix carbon through photosynthesis and help decrease levels of atmospheric CO<sub>2</sub> [2]. In addition, shading and transpiration of street trees can reduce high urban temperatures and improve the thermal comfort for humans [1,4]. Atmospheric

particle pollution has become a serious health issue globally, and PM<sub>2.5</sub>, fine particles with a diameter of 2.5 µm or less, is one of the main atmospheric pollutants. Urban vegetation has the ability to take in the pollutants. Compared with shorter vegetation, trees can capture fine particles more effectively, and thus improve air quality in urban areas [3,5–9]. Better air quality and local climates can provide a more comfortable residential environment, and the visual effects of street trees will affect people's perception of the environment [10]. Apart from the above benefits, street trees have some other instrumental functions, such as noise pollution mitigation [10], aesthetic improvement [3,6–9], urban biodiversity conservation, human health improvement [8,9], building energy reduction [4], and surface water runoff reduction [5,7].

Street trees are integral to urban forests, and they are able to provide ecosystem services for urban ecosystems. In order to understand the functions that urban forests (including street trees) provide, several specific quantified values are used to assess these functions. Dobbs et al. [11] integrated some indicators (CO<sub>2</sub> sequestration by trees, air pollutants removal, tree structure, crown dieback) into a framework to monitor the functions of urban forests. Moreover, many studies and researches have been conducted to assess the urban ecosystem services, including air pollutants removal [12–15], carbon storage and sequestration [14,16,17], and climate change mitigation and adaptation [16]. Urban Forest Effects (UFORE) model, which is developed by United States Department of Agriculture, can help assess the urban forest structure and its functions [18], and the model has been integrated into a software application, i.e., i-Tree Eco, to make assessments more convenient. Nowak et al. [13] combined i-Tree Eco model and field data on trees to determine the leaf surface area within 10 U.S. cities, and help evaluate the amount of PM<sub>2.5</sub> removed by urban trees. Apart from the U.S., the i-Tree Eco model can be applied in other countries as well. For instance, Kiss et al. [14] used the model to evaluate carbon sequestration and air pollution removal based on the ecological processes of street and park trees in Szeged city, and Selmi et al. [15] quantified the air pollution removal by urban trees in Strasbourg city by utilizing the i-Tree Eco model. Referring to other tools and methods is another option to assess some functions. Chen et al. [12] used the atmospheric particle sampler TH-3150 and the gravimetric method to measure PM<sub>10</sub> concentrations, and evaluated the efficiency of greenbelts in removing PM<sub>10</sub> by comparing the PM<sub>10</sub> concentrations at non-greenbelts and behind the greenbelts. Nowak et al. [17] utilized biomass equations to estimate carbon storage of different kinds of urban trees. Carbon sequestration estimation needs the additional measured tree growth rates.

Biomass directly relates to the tree structure, including tree height and diameter at breast [19], which is critical to evaluating the ecosystem services of both natural forests and urban forests. Additionally, biomass is essential for carbon stock estimate [20], and thus biomass quantification is of great help to evaluate carbon sequestration.

Acquiring biomass measurements with high accuracy usually requires analyzing trees in a destructive way, which is labor- and time-intensive [21]. LiDAR (Light Detection and Ranging), also called laser scanning, is a method that can acquire 3D information of objects through a LiDAR system, which consists of laser scanners, global positioning system (GPS), and inertial measurement unit (IMU). According to the platforms that laser scanning systems are mounted on, they can be categorized as airborne laser scanning (ALS), terrestrial laser scanning (TLS), and mobile laser scanning (MLS). ALS has laser scanning systems mounted on aircrafts, such as planes and unmanned aerial vehicles (UAV). Platforms for TLS are tripods, which are immobile during data acquisition process. For MLS, laser scanning systems are usually mounted on moving vehicles, including cars and trucks [22]. Laser scanning provide a non-destructive way to quantify biomass, which can replace the costly methods based on field measurements [23]. ALS and TLS have been widely applied to forestry, including tree canopy structure characterization, aboveground forest biomass estimation, structural parameters measurements, forest structural attributes and carbon stock estimation [21,23–28]. Biomass estimation of vegetation is a common application of laser scanning. Greaves et al. [21] estimated biomass of two shrub species, dwarf birch and diamond-leaf willow, in Arctic tundra by using TLS data. Ene et al. [27] combined various sampling strategies and ALS measurements to estimate aboveground biomass

(AGB) in miombo woodlands. Moreover, laser scanning is applied not only at plot level, but also at individual tree level. For example, Kankare et al. [29] developed models which are based on TLS data to estimate AGB of individual trees, and AGB estimation accuracies were improved when comparing with existing models. Laser scanning data can also be applied to evaluate carbon stocks in forests. Coomes et al. [26] compared the results of two different forest carbon mapping methods, an area-based method and a tree-centric method, by using the ALS point clouds. Above studies indicate that current applications of laser scanning mainly focus on natural forests, and few researches have been conducted for urban forests, especially for street trees.

ALS and TLS can be applied to different situations because of their own features. TLS is an efficient choice for acquiring accurate field data and is able to measure all important tree parameters [29]. TLS is more likely to carry out investigations at individual tree level. When trees in different plots need to be surveyed, TLS may suffer from laborious relocations [30]. As for ALS, it has relatively low point density that cannot depict canopy structure precisely, and thus ALS is usually utilized for plot level estimations of tree characteristics [30,31]. Unlike ALS and TLS, MLS is seldom used for forestry applications. MLS can hardly move in natural forests, but it has incomparable superiority in urban applications, particularly in road inventory investigation [31]. MLS systems are more efficient than TLS systems and MLS data have higher point density than ALS data. The information of street trees can be recorded easily and comprehensively with MLS systems moving along the streets.

The objective of this study was to evaluate carbon sequestration and PM<sub>2.5</sub> removal by using MLS data and meteorological data, including wind speed and local PM<sub>2.5</sub> concentrations. We investigated (1) the method of extracting point cloud data of individual trees from raw MLS data; (2) the approach to measure tree morphological parameters, including tree height, crown width, and diameter at breast height, with the point clouds of individual trees; (3) the evaluation of carbon sequestration and PM<sub>2.5</sub> removal for various tree species based on the measured parameters and ecological models. According to the results, we also compared the ability of several tree species to sequester carbon and intercept PM<sub>2.5</sub>.

## 2. Materials

### 2.1. Study Area

Field data and MLS data were collected for three streets, namely Bihua Street, Taihu Street, and Shuangxia Street, in Nantong city (32°4'24" N, 121°5'27" E), which are located in the southeast of Jiangsu province (Figure 1). Nantong has a temperate climate and mean precipitation in this city is approximately 1040 mm, and annual mean temperature in Nantong is around 15.1 °C. Nantong has various species of street trees, including *Platanus acerifolia*, *Cinnamomum camphor* (L.) Presl and *Sapindus mukurossi* Gaertn. The investigated streets have four different tree species. Street trees of Bihua Street are *Platanus acerifolia* and *Cinnamomum camphor* (L.) Presl, and street trees of Taihu Street and Shuangxia Street are *Sapindus mukurossi* Gaertn and *Acer mono Maxim.* respectively.

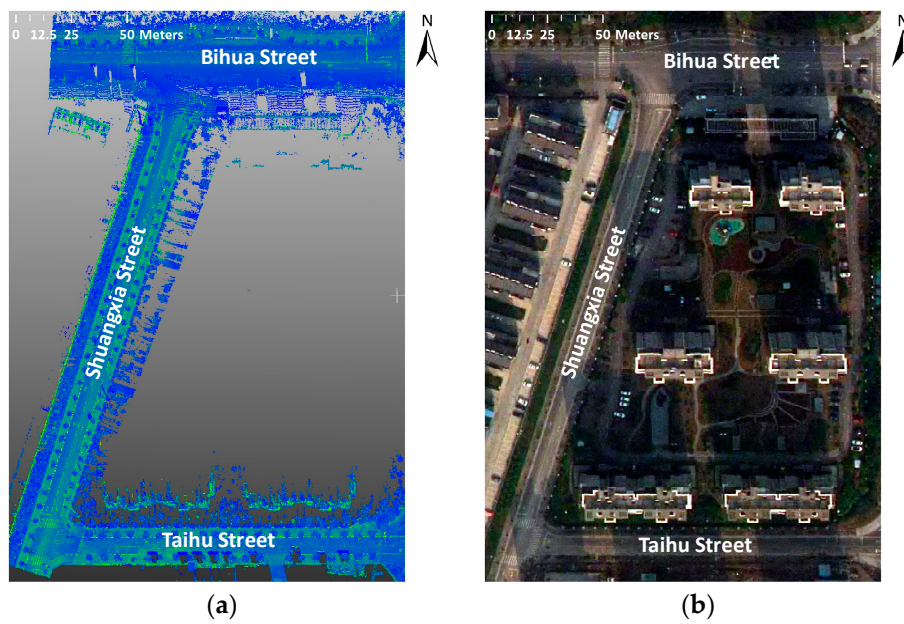


Figure 1. Study area in Nantong City. (a) Point cloud data; (b) Aerial image.

2.2. Data Collection and MLS System

MLS data of the three streets were collected in May 2015, while field data of these streets were collected in July 2015. Specific information of street trees, including tree species, DBH, tree height, crown width, and precise position, were obtained during field data acquiring process. Point cloud data were collected by a HiScan-Z mobile laser scanning system (hereafter referred to as the “MLS”, Figure 2, Table 1), which is produced by Hi-Cloud Company, with high precision. MLS scans were performed when the system moved along the streets. Objects, such as buildings, trees, street lamps, and road signs, were scanned and their detailed information was recorded.

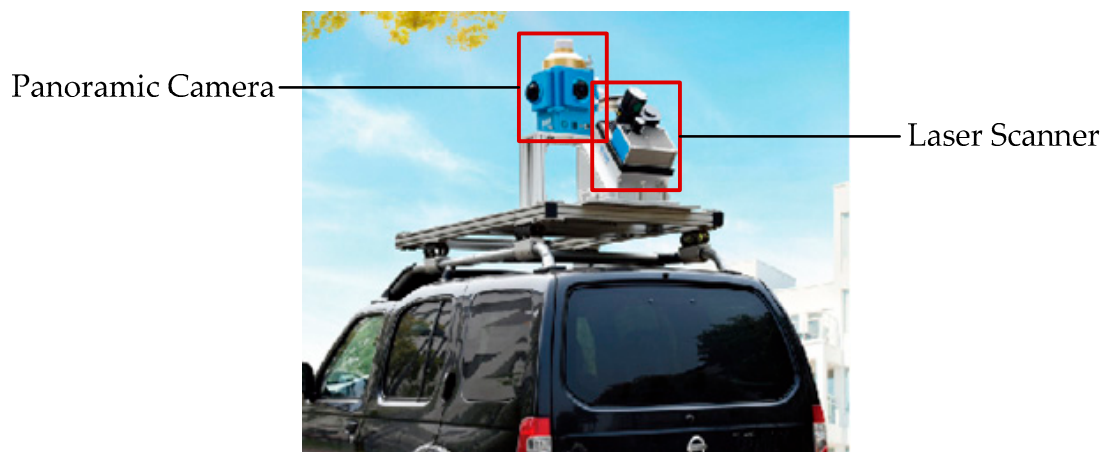


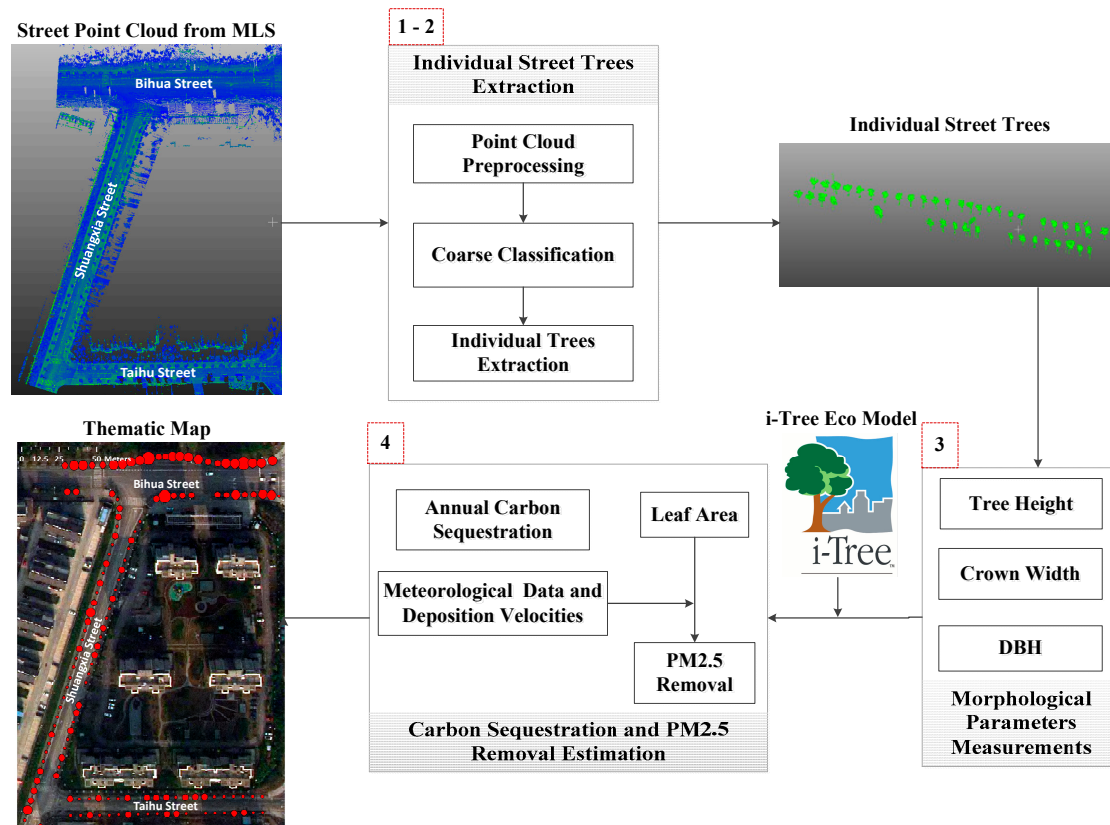
Figure 2. HiScan-Z mobile laser scanning system.

Table 1. HiScan-Z laser scanning system technical specifications.

Measurement distance	119 m
Laser transmitting frequency	1,010,000 points per second
Ranging precision	0.9 mm @ 50 m
Field of view	360°
Panoramic camera	Ladybug/HD camera (optional)
Panoramic resolution	30,000,000/75,000,000 pixels

### 3. Methods

The method (Figure 3) proposed in this study consists of four steps, which are coarse classification of point cloud data, individual street trees extraction, morphological parameters measurements, and carbon sequestration and PM<sub>2.5</sub> removal estimation, respectively.



**Figure 3.** Flow chart of evaluating carbon sequestration and PM<sub>2.5</sub> removal of street trees with MLS data.

#### 3.1. Individual Street Trees Point Clouds Extraction

A range of methods have been applied to detect individual trees in both natural forests and urban forests with point cloud data. Some of these methods choose not to process point cloud data directly, and use other LiDAR-derived data instead, such as Canopy Height Model (CHM), to extract single trees [32]. In recent years, methods [33–35] for extracting urban objects based on MLS data have developed rapidly. In this paper, we presented a simpler method (Figure 4) that used point cloud vertical characteristics and unique structural features of trees to extract individual street trees.

##### 3.1.1. MLS Data Preprocessing

When we obtained raw MLS data, some preprocessing measures were taken. First of all, ground points and non-ground points were separated by utilizing the Cloth Simulation Filter (CSF), which is proposed by Zhang et al. [36]. The CSF algorithm assumes that there is a cloth covering the inverted point clouds, and the cloth would become an approximation of the ground surface. Ground points in point clouds can be extracted by comparing the generated cloth surface and the original LiDAR points. Then, noise and outlier points were removed by noise filter and Statistical Outlier Removal (SOR) filter. The SOR filter conducts statistical analysis for points in point clouds. For each point, the SOR filter computes the average distance to its neighbors, and if the distance is not within a certain

range, the point will be regarded as an outlier and be removed from point clouds. When the above two procedures finished, the continuity of objects was broken and noise points were removed.

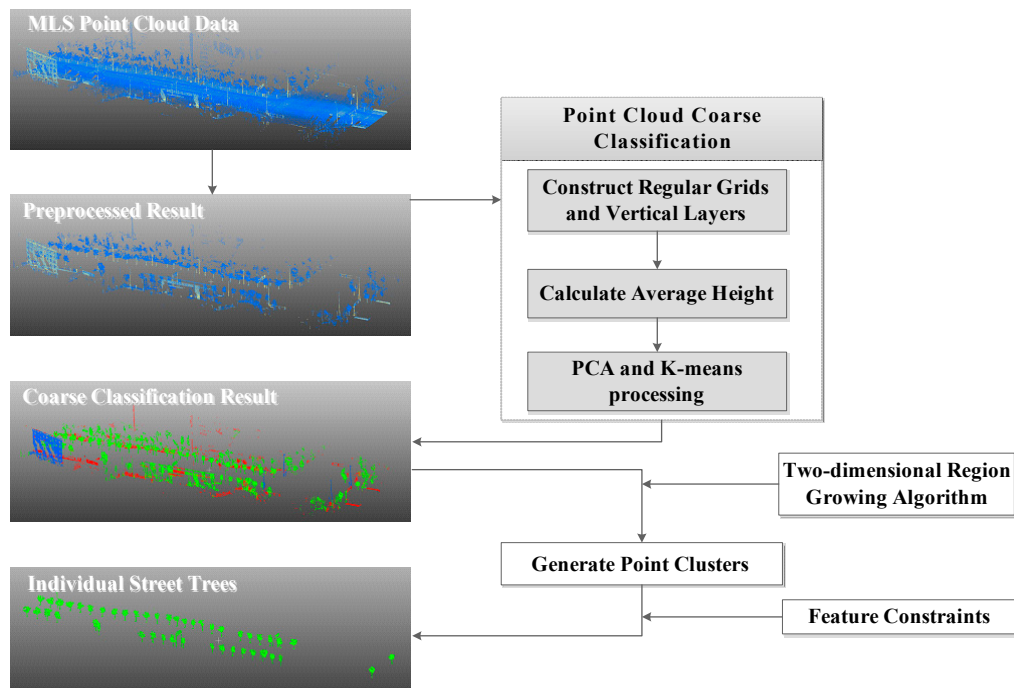


Figure 4. The process of extracting individual street trees.

### 3.1.2. Point Clouds Coarse Classification

After MLS data were preprocessed, the remaining points could be categorized as buildings, vegetation, road facilities, and some other ground objects. Generally, objects in these categories have different average heights. Vegetation that close to ground, such as shrubs or grass, are usually the lowest ground objects, street lamps and street trees have medium height, and buildings have the largest average height (Figure 5). Coarse point cloud classification was conducted based on this perception, and coarse classification could eliminate points of ground objects whose heights were higher or lower than street trees. Algorithm 1 presents the process of point clouds coarse classification.

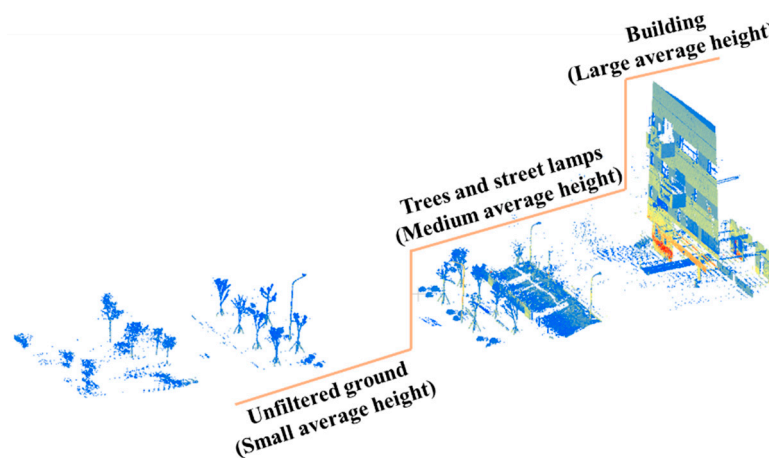


Figure 5. Average heights of different ground objects.

**Algorithm 1.** Point clouds coarse classification algorithm

**Input:** Filtered MLS point clouds  $P_1 = \{(X_i, Y_i, Z_i) \mid i = 1, 2, \dots, n, n \text{ is the number of points}\}$

**Output:** Point clouds with classification information  $P_2 = \{(X_i, Y_i, Z_i, c_j) \mid i = 1, 2, \dots, n, n \text{ is the number of points; } c_j \text{ is class number, } j = 1, 2, \dots, m, m \text{ is the number of classes}\}$

1. Set cubic square grids for points and put points into corresponding grids (Figure 6). The size of grid is set as  $l \text{ m} \times l \text{ m} \times h \text{ m}$ , and the value of  $l$  is set manually while the value of  $h$  is determined according to Equation (1).
2. Stratify points in each grid into layers with a proper spacing ( $S$ ) (Equation (2), Figure 6) and calculate the average height of points in each layer (Equation (3)). Generally,  $S$  can be different for various situations, but it cannot be overly large or small. For most situations,  $1\text{m}$  is a proper value for  $S$ .
3. Construct an  $m \times n$  ( $m$  is the number of grids,  $n$  is the number of layers in each grid (Equation (4))) matrix and each  $n \times 1$  vector represents the average heights array of the corresponding grid (Figure 6).
4. Utilize Principal Component Analysis (PCA) to reduce dimensions of the matrix and get the matrix's dominant features.
5. Use K-means algorithm to complete the classification of the vectors, and points that correspond to vectors, would also find their class. Add classification number,  $c_j$ , for each point.
6. Return:  $P_2$ .

$$h = Z_{\max} - Z_{\min} \quad (1)$$

where  $Z_{\max}$  and  $Z_{\min}$  are the maximum and the minimum value of  $Z$  coordinates.

$$V_i = \text{int}\left(\frac{Z_i}{S}\right) \quad (2)$$

where  $S$  is the layer spacing, the point  $(X_i, Y_i, Z_i)$  is in the  $V_i$ th layer.

$$\bar{H} = \begin{cases} \frac{Z_1 + Z_2 + Z_3 + \dots + Z_n}{n} & (n \neq 0) \\ 0 & (n = 0) \end{cases} \quad (3)$$

where  $n$  is the number of points in the layer.

$$n = \text{int}\left(\frac{h}{S}\right) + 1 \quad (4)$$

where  $n$  is the number of layers in each grid,  $S$  is the layer spacing and  $h$  is the height of the cubic square grid.

According to the complexity of the ground objects in the study area, preprocessed MLS data were finally classified into three or four classes on the basis of average heights of point cloud data. The class that contained street trees would be processed in the next procedure.

### 3.1.3. Individual Street Trees Extraction

Since point cloud data became disconnected point blocks, points could cluster into independent ground objects based on spatial relations between points. Individual street trees could be extracted by selecting point clusters that had specific features.

The class which contained street trees was selected, and regular cubic square grids were set for this class with a smaller grid spacing,  $0.2 \text{ m} \times 0.2 \text{ m}$ . The number of points in each grid was counted. According to the fact that whether the grid had points, we generated a table with  $n_x \times n_y$  cells ( $n_x$  is the number of rows,  $n_y$  is the number of columns). If one grid had points, the value of its corresponding cell would be set as the number of points, otherwise the value would be set as zero (Figure 7).

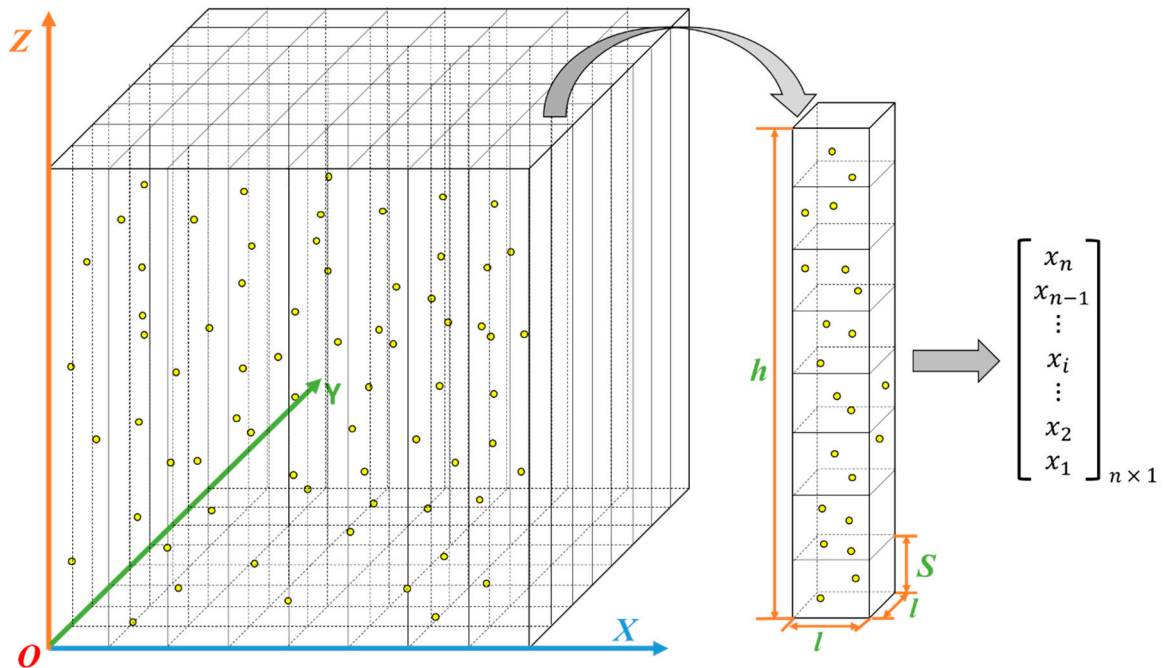


**Figure 6.** The process of setting cubic square grids for points, stratifying each grid into layers, and constructing vectors for grids.

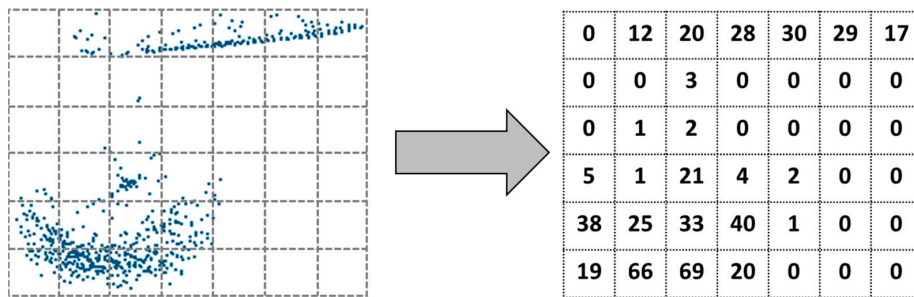


**Figure 7.** Generate a table that records the number of points in each grid. The image on the left is the top view of some cubic square grids, and the image on the right is the table corresponds to these cubic square grids.

Then, the table was divided into different parts by using a two-dimensional region growing algorithm (Algorithm 2, Figure 8). In Algorithm 2,  $P_{seed}$  is a set that reserves seed cells.

---

**Algorithm 2.** Two-dimensional region growing algorithm

---

**Input:**  $T_a$ , a table that records the number of projected points in each grid (Figure 8a).

**Output:**  $T_b$ , a table whose cells are clustered into different parts (Figure 8d).

---

1. Traverse  $T_a$  and find an unmarked valid cell, whose value is not zero, and mark the cell as a seed cell. Put the cell into  $P_{seed}$ .
  2. Select a cell from  $P_{seed}$ ,  $S_i$ , mark the cell and erase it from  $P_{seed}$ .
  3. Search four adjacent cells (in order of up, down, left and right) around  $S_i$ . If adjacent cells were valid, these cells would be put into  $P_{seed}$ .
  4. Loop process 2 to 3 until  $P_{seed}$  is empty, and marked cells would cluster into one part.
  5. Go back to process 1 to find a new seed cell, and conduct process 2 to 4 sequentially until all valid cells are marked.
  6. Return:  $T_b$ .
-



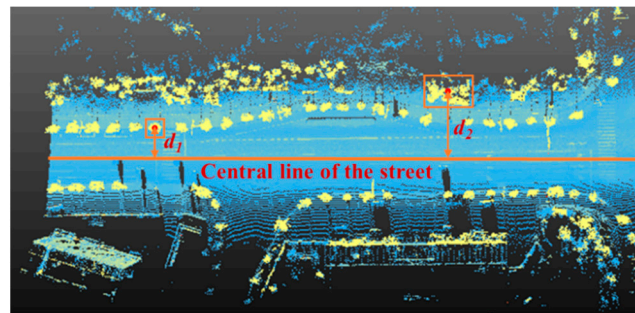


Figure 9. Distances between ground objects and the central line of the street.

Values of  $\Delta Z$ ,  $\Delta X/\Delta Y$ ,  $PA$ , and  $d$  of all point clusters would be calculated, and constraints of these values would be set (Table 2). The  $\Delta Z$  threshold was set as 1.3 m because heights of most street trees were above 1.3 m. Given that point clouds of street trees were not complete and the integrity of tree crowns was damaged,  $\Delta X/\Delta Y$  was set between 0.5 and 1.5 to avoid omitting some trees.  $PA$  of street trees varied and it was hard to choose proper thresholds. In this case, several experiments were conducted before determining thresholds of  $PA$ , and the final minimum threshold and maximum threshold were 60 and 300. Distances from street trees to street central line were restricted between  $(SW/2-1)$  m to  $(SW/2+1)$  m to provide buffer for the distances. When point clusters can satisfy all constraints, these point clusters would be eventually extracted as street trees.

Table 2. Feature constraints for point clusters.

$\Delta Z$	$\Delta X/\Delta Y$	$PA$	$d$
$\Delta Z > 1.3$ m	$0.5 < \Delta X/\Delta Y < 1.5$	$60 < PA < 300$	$(SW/2-1)$ m $< d < (SW/2+1)$ m

SW: Street width.

### 3.2. Morphological Parameters of Trees' Measurements

The application of laser scanning technology can acquire precise information of urban trees rapidly and reduce the workload for urban forest workers. Various algorithms [34,37,38] for measuring morphological parameters with different kinds of laser scanning data, including ALS data, TLS data, and MLS data, have been studied. In this study, we primarily measured three morphological parameters of trees, including tree height, crown width, and DBH. To make the measuring process more specific, points of crown and trunk were separated.

#### 3.2.1. Tree Height Measurement

Tree height measuring method was conducted with following steps:

Step 1: Project trunk points onto the  $XOY$  plane, and fit these projected points with a circle [39], whose center is  $(X_0, Y_0)$ .

Step 2: Construct a square that regards  $(X_0, Y_0)$  as its center. The length and width of the square are set as 1.5 m to contain points around the trunk.

Step 3: Find projected points that are in the square, namely their coordinates  $(X, Y)$  satisfy Expression (7), and extract their corresponding 3D points.

$$X_0 - 0.75 \leq X \leq X_0 + 0.75 \quad Y_0 - 0.75 \leq Y \leq Y_0 + 0.75 \quad (7)$$

Step 4: Measure the tree height by calculating the difference between the maximum  $Z$  coordinate and the minimum  $Z$  coordinate of the extracted 3D points.

The measuring method employed in this study considers points in the primary growing direction.

### 3.2.2. Crown Width Measurement

Crown points were selected to measure crown width by following the steps below (Figure 10):

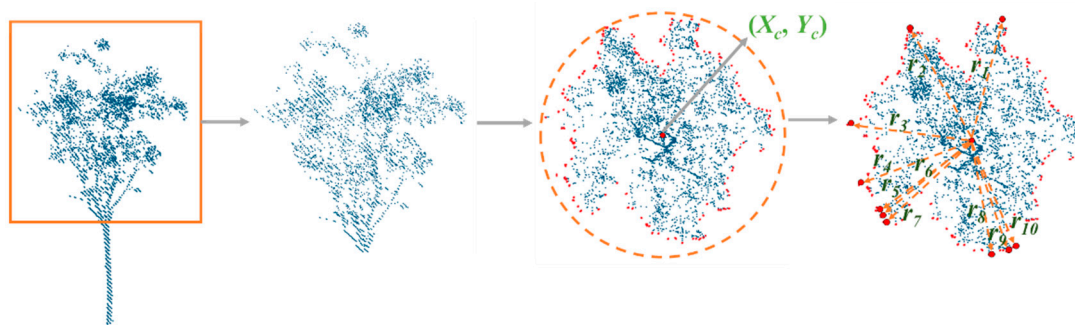


**Figure 10.** Crown width measuring method.

Step 1: Project crown points onto the horizontal plane ( $XOY$  plane), and extract boundary points of projected crown points.

Step 2: Find the minimum circle that enclose all crown boundary points, and obtain the coordinates of the circle's center,  $(X_c, Y_c)$ .

Step 3: Calculate distances ( $L$ ) between boundary points and the center of the circle (Equation (8)). The average of ten largest distances is regarded as half of the crown width (Equation (9)).

$$L = \sqrt{(X - X_c)^2 + (Y - Y_c)^2} \quad (8)$$

$$\frac{CW}{2} = \frac{r_1 + r_2 + r_3 + r_4 + r_5 + r_6 + r_7 + r_8 + r_9 + r_{10}}{10} \quad (9)$$

### 3.2.3. DBH Measurement

For trees with different point density, two DBH measuring methods were introduced in this study:

(1) For trees with relatively high point density, trunk points between 1.2 m to 1.4 m off the ground are extracted and a circle is fitted for these points. The diameter of the circle is regarded as DBH.

(2) For trees whose trunk points at breast height are sparse and cannot depict the profile of the trunk, all trunk points are employed to measure DBH. Trunk points are segmented vertically with a proper spacing, 0.2 m to 0.4 m. Points in each segment would be projected onto the horizontal plane and a fitted circle would be formed for the points in the segment. The average of diameters of all circles is DBH (Equation (10)).

$$DBH = \frac{d_1 + d_2 + \dots + d_n}{n} \quad (10)$$

where  $n$  is the number of trunk segments.

### 3.3. Carbon Sequestration Estimation

Biomass of each street tree can be calculated by using allometric equations, and whole tree dry weight biomass and carbon storage can be estimated with conversion factors [17]. Thus, before estimating carbon storage of street trees, their biomass needs to be calculated first, and tree height and DBH are applied in allometric equations to estimate biomass. Annual carbon sequestration of street trees is the difference of their carbon storage between year  $x$  and year  $(x+1)$ . So, tree height growth and DBH growth in a year would be predicted before estimating carbon sequestration [17]. In this research, the i-Tree Eco model was employed to calculate carbon sequestration. Essential information of street trees was imported to i-Tree Eco software, and detailed calculating results, including leaf area, carbon storage, and annual gross carbon sequestration, of each street tree were obtained.

### 3.4. PM<sub>2.5</sub> Removal Estimation

UFORE-D, a part of UFORE model and specializing in estimating air pollution removal, was employed to estimate PM<sub>2.5</sub> removal in our study. Equation (11) [13] is the calculating formula of hourly pollution removal:

$$F = V_d \times C \quad (11)$$

where  $F$  ( $\mu\text{g}\cdot\text{m}^{-2}\cdot\text{h}^{-1}$ ) is the deposition flux,  $V_d$  ( $\text{m}\cdot\text{h}^{-1}$ ) is the deposition velocity of pollutants to the leaf surface and  $C$  ( $\mu\text{g}\cdot\text{m}^{-3}$ ) is the pollutant concentration. Total removal of PM<sub>2.5</sub> can be calculated according to Equation (12) [40]:

$$M = F \times LA \times T \quad (12)$$

where  $M$  is the total quantity of PM<sub>2.5</sub> removal,  $LA$  is leaf area of street trees and  $T$  is the number of purifying hours. To estimate PM<sub>2.5</sub> removed by street trees, leaf area of street trees, PM<sub>2.5</sub> concentration monitoring data, and daily purifying hours need to be collected. Leaf area [41] is calculated by using the i-Tree Eco model, and PM<sub>2.5</sub> concentration data and daily purifying hours can be obtained by visiting the meteorological website. Apart from these data, the deposition velocity of PM<sub>2.5</sub> to the leaf surface ought to be determined. The deposition velocity is determined by experiments instead of experiential research, and because of the restricted experimental conditions, we referred to some references to find corresponding deposition velocities of PM<sub>2.5</sub> for different tree species. Table 3 [13,40] presents deposition velocities of several tree species at different wind speeds. Deposition velocities for four tree species in our research could not be found in the references, so deposition velocities of *Cinnamomum camphor* (L.) Presl and *Acer mono Maxim.* were replaced by average deposition velocities of evergreen broadleaved trees and deposition velocities of *Acer pseudoplatanus*, respectively, and deposition velocities of *Sapindus mukurossi Gaertn* and *Platanus acerifolia* were replaced by average deposition velocities of deciduous broadleaved trees.

**Table 3.** Deposition velocities ( $\text{cm}\cdot\text{s}^{-1}$ ) of PM<sub>2.5</sub> at different wind speed per unit leaf area.

Tree Species	Wind Speed ( $\text{m}\cdot\text{s}^{-1}$ )		
	3	6	8.5
<i>Cinnamomum camphor</i> (L.) Presl	0.03	0.06	0.16
<i>Acer mono Maxim.</i>	0.042	0.197	0.344
<i>Platanus acerifolia</i>	0.25	0.63	1.19
<i>Sapindus mukurossi Gaertn</i>	0.25	0.63	1.19

## 4. Results

Extraction of individual street trees was applied for three streets in the study area, respectively, and the extracting correctness rates were above 92%. Morphological parameters of each street tree were calculated and the results were evaluated by comparing with the field-measured parameters. With the employment of the i-Tree Eco model and morphological parameters, carbon sequestration and PM<sub>2.5</sub> removal were estimated.

### 4.1. Street Trees Extraction

During MLS data acquiring process, data of three streets were collected separately, thus street trees extraction for streets were performed individually.

Before conducting coarse classification, the square grid size and the layer spacing needed to be determined. In order to find appropriate grid size, layer spacing, and the number of classes, we attempted different combinations of these three parameters. Final combinations for the three streets were shown in Table 4. Bihua Street and Shuangxia Street had the same grid size and layer spacing, while these two parameters of Taihu Street were slightly larger. The final grid sizes,  $4\text{ m} \times 4\text{ m}$  and  $5\text{ m} \times 5\text{ m}$ , were close to the sizes of street trees' crowns. By observing ground objects on the three

streets, we found that there was no building on Shuangxia Street, and buildings on Taihu Street were higher than buildings on Bihua Street. In addition, Taihu Street had more abundant variety of ground objects than other two streets. Therefore, Taihu Street needed a larger layer spacing (2 m), and more classes (4 classes). With the final parameters setting, most street trees were classified into the same class. Then, points in the class, which contained street trees, were allocated to different point clusters. When a point cluster met all requirements presented in Table 2, the point cluster would be extracted as a street tree.

**Table 4.** Grid size, layer spacing, and the number of classes for coarse classification.

Streets	Grid Size (m)	Layer Spacing (m)	Number of Classes
Bihua St.	4 × 4	1	3
Shuangxia St.	4 × 4	1	3
Taihu St.	5 × 5	2	4

Results of street trees extraction are presented in Table 5. Extraction completeness rates for Bihua Street, Shuangxia Street, and Taihu Street were 97.9%, 98.4%, and 100% respectively, and correctness rates for these three streets were 92%, 98.4%, and 93.2% respectively. Figure 11 showed false extraction results by using the proposed algorithm, including false positives and false negatives. Some street lamps and road signs, whose point clouds mixed with street trees, were extracted as street trees. Trees with lower tree heights and smaller crown widths were omitted by the algorithm. Figure 12 presents the extraction results of the three streets in the study area.

**Table 5.** Street trees extraction results.

Streets	Results	Extracted Street Trees	Omitted Street Trees	Extracted Other Ground Objects	Completeness Rate	Correctness Rate
Bihua St.		46	1	4	97.9%	92%
Shuangxia St.		61	1	1	98.4%	98.4%
Taihu St.		41	0	3	100%	93.2%

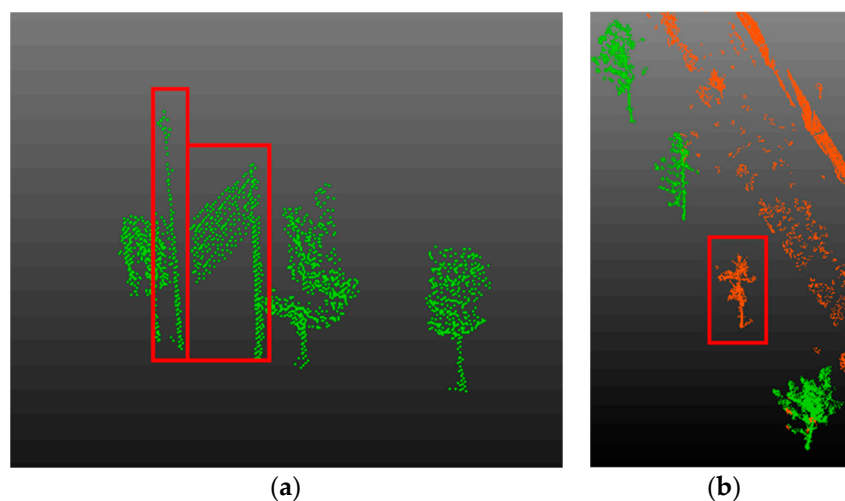


**Figure 11.** False extraction results generated by the proposed method. (a) False positives; (b) False negative.

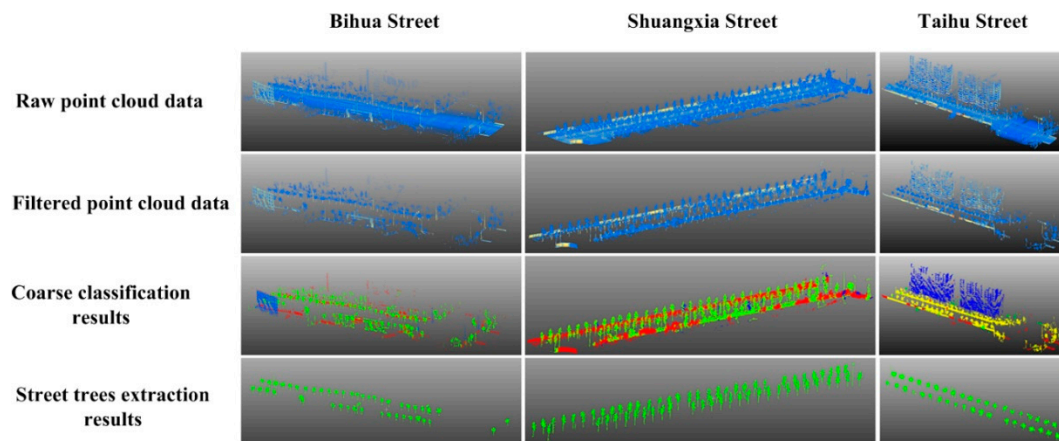


Figure 12. Extracting street trees from raw point cloud data.

#### 4.2. Morphological Parameters Measurements

In total, there were 148 street trees extracted from MLS data. Some street trees were not in study area and field data of these trees were not collected, so we excluded these trees and extracted the omitted street trees manually. Eventually, morphological parameters for 143 street trees were measured. The number of street trees on Bihua Street, Shuangxia Street, and Taihu Street was 41, 62, and 40, respectively.

For street trees on each street, *RMSE* (Root Mean Square Errors) and mean errors of the three morphological parameters were calculated (Table 6). Parameters of street trees on Taihu Street had the largest *RMSE* of tree height and crown width, while the *RMSE* of DBH was the smallest. Street trees on Bihua Street had the smallest *RMSE* of crown width measurements and the largest *RMSE* of DBH measurements. *RMSE* of tree height measurements for street trees on Shuangxia Street was the smallest. Although *RMSE* of morphological parameters measurements for trees on the three streets differed, the differences were minor. Values of mean errors of these parameters' measurements indicated that morphological parameters derived from MLS data were mostly underestimated.

Table 6. RMSEs and mean errors for morphological parameters of each street.

Streets	Parameters	Tree Height (m)		Crown Width (m)		DBH (cm)	
		RMSE	Mean Error	RMSE	Mean Error	RMSE	Mean Error
	Bihua St.	0.12	−0.08	0.24	−0.14	2.12	−1.10
	Shuangxia St.	0.11	0.10	0.26	−0.01	1.95	−0.31
	Taihu St.	0.17	−0.03	0.37	−0.05	1.85	−0.32

To understand the relevance between MLS-derived parameters and field measured parameters, scatter plots were created for the three parameters (Figure 13).  $R^2$  values for tree height and crown width are 0.99 and 0.80, respectively, while  $R^2$  for DBH is 0.52. Due to the issue of tree trunks point density, measurements of DBH is more difficult and complicated, and MLS-derived DBH is less correlated with field measured DBH. Tree heights of street trees ranging from 4 m to 10 m, and this parameter showed a better agreement between MLS-derived results and field measured results than the other two parameters. Trees on Shuangxia Street had larger tree heights than trees on Bihua Street and Taihu Street. Crown widths were between 1.5 m and 5 m, and street trees on Taihu Street had larger average crown width. As for DBH, most street trees had DBH ranging from 7.5 cm to 20 cm, only a tree on Bihua Street had DBH approximated to 25 cm. Overall, morphological parameters derived from MLS data had relatively high accuracy.

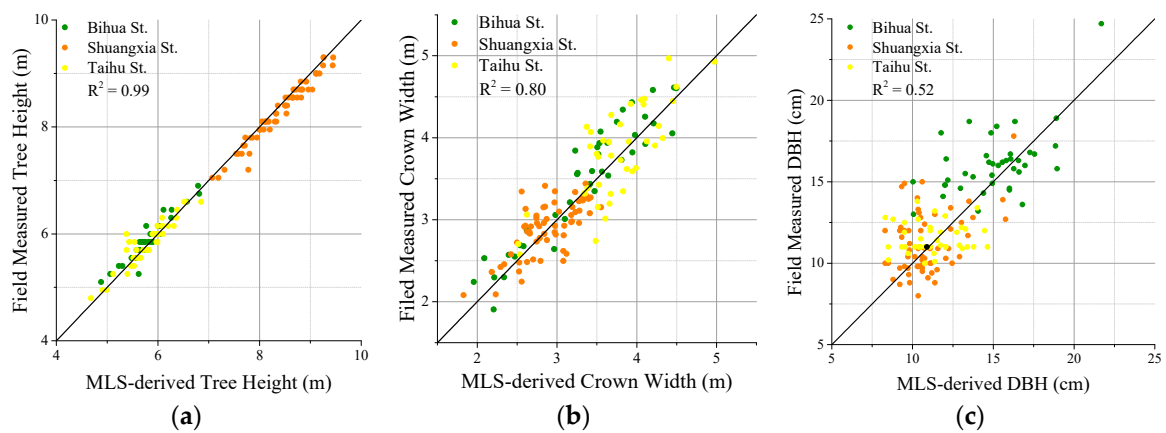


**Figure 13.** Comparison between MLS-derived morphological parameters and field measured morphological parameters. (a) Tree height; (b) Crown width; (c) DBH.

#### 4.3. Carbon Sequestration and $PM_{2.5}$ Removal Estimation

Measured morphological parameters of each street tree were imported to the i-Tree Eco model to estimate carbon sequestration and  $PM_{2.5}$  removal.

Annual carbon sequestration (Figure 14a) could be obtained directly from reports that generated from i-Tree Eco software. Carbon sequestration of street trees ranged from 1.2 kg/year to 5.2 kg/year. *Cinnamomum camphor* (L.) Presl trees on Bihua Street had the largest annual carbon sequestration. Several *Acer mono Maxim.* trees on Shuangxia Street and *Sapindus mukurossi Gaertn* trees on Taihu Street had relatively large annual carbon sequestration, while the rest of *Acer mono Maxim.* trees, *Sapindus mukurossi Gaertn* trees and a *Platanus acerifolia* tree on Bihua Street had less annual carbon sequestration.

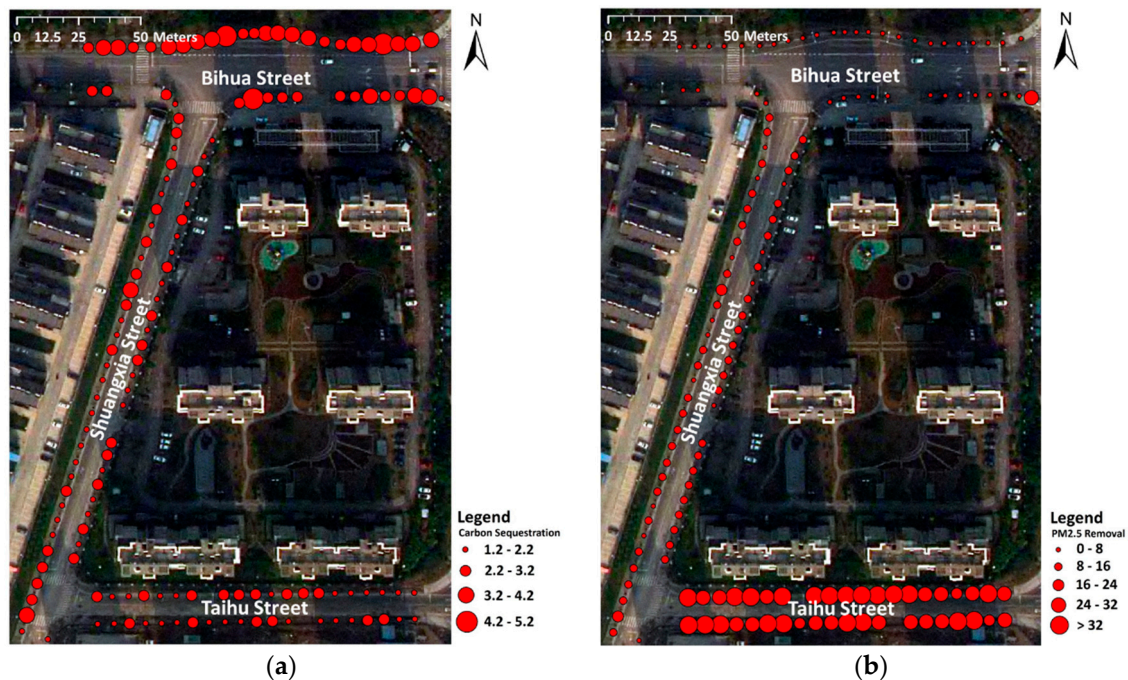


**Figure 14.** Annual carbon sequestration and  $PM_{2.5}$  removal of each street tree. (a) Annual carbon sequestration of street trees; (b)  $PM_{2.5}$  removed by street trees in April 2015.

As for  $PM_{2.5}$  removal (Figure 14b), we collected meteorological data, including  $PM_{2.5}$  concentrations and wind speeds (Table 7), in April 2015 of Nantong. There were 10 rainy days in April 2015 and these days were excluded in our research, so the total purifying time was 20 days.

PM<sub>2.5</sub> removed by street trees in April 2015 ranged from 2 g to 43 g. *Sapindus mukurossi Gaertn* trees on Taihu Street and the *Platanus acerifolia* tree on Bihua Street had large PM<sub>2.5</sub> removal, while *Cinnamomum camphor* (L.) Presl trees on Bihua Street had less PM<sub>2.5</sub> removal. The amount of PM<sub>2.5</sub> that removed by *Acer mono Maxim.* trees was between the amount of PM<sub>2.5</sub> removed by *Sapindus mukurossi Gaertn* trees and *Cinnamomum camphor* (L.) Presl trees. The distribution of PM<sub>2.5</sub> removal was significantly different from the distribution of annual carbon sequestration.

**Table 7.** PM<sub>2.5</sub> concentrations and wind speeds of Nantong in April 2015.

Date	4.1	4.3	4.8	4.9	4.10	4.11	4.14	4.15	4.16	4.17
PM <sub>2.5</sub> concentration (μg·m <sup>-3</sup> )	75	54	37	36	44	52	59	77	75	31
Wind speed (m·s <sup>-1</sup> )	6	3	3	3	3	3	8.5	6	6	8.5
Date	4.20	4.21	4.22	4.23	4.24	4.25	4.26	4.27	4.29	4.30
PM <sub>2.5</sub> concentration (μg·m <sup>-3</sup> )	38	52	89	90	79	103	66	51	27	61
Wind speed (m·s <sup>-1</sup> )	8.5	3	3	3	3	3	6	8.5	3	3

## 5. Discussion

### 5.1. Street Trees Extraction

To complete street trees extraction, point clouds coarse classification and extracting individual street trees based on feature constraints need to be accomplished.

For coarse classification, setting the grid size and the layer spacing is a critical step, because these two parameters have direct influences on classification results. Several combinations of these two parameters were employed to obtain satisfactory coarse classification results. However, regular grids sometimes cannot obtain integral trees and this problem would generate some errors when measuring morphological parameters of trees. When extracting individual street trees, four feature constraints, including three morphological feature constraints ( $\Delta Z$ ,  $\Delta X/\Delta Y$ ,  $PA$ ) and a positional feature constraint ( $d$ ), are proposed. Morphological features of point clusters can assist to depict the shapes of trees. Constraining the morphological features can exclude some ground objects whose morphological features do not match to trees, such as walls, street lamps, and road signs. The positional feature constraint,  $d$ , is restricted to about half of the street width ( $SW$ ) to help eliminate trees that are not street trees.

Most street trees on the three streets were successfully extracted based on coarse classification and feature constraints. Nevertheless, some trees were omitted and a few street lamps and road signs were difficult to remove. As the coarse classification is conducted based on average heights of ground objects, trees whose height were much lower or higher than the average height of all trees may be omitted. If street trees had irregular shapes or small crowns so that they could not satisfy feature constraints, these trees were omitted as well. Street lamps and road signs, whose point clouds mixed with street trees, could be hard to distinguish from street trees, and the proposed method could not deal with the situation at present. Our method needs to be improved to separate mixed point clouds.

Currently, many methods consider using 3D voxels and spatial region growing algorithms [34,35,42] to obtain point clouds of street objects from MLS data, including street trees, more accurately. This kind of method can acquire more accurate extraction results, but also requires lots of computing resources. Moreover, Tao et al. [43] introduced the comparative shortest-path algorithm (CSP) which utilized metabolic ecology theories to segment tree crowns. Utilizing ecological theories to segment trees is considerably novel and can make use of ecological features of trees. Lehtomäki et al. [44] proposed a machine-learning-based method to complete street objects classification. Completeness and correctness of street objects classification and extraction are improved attributing to the method. Our method can extract street trees correctly and efficiently for simple street environment. However, the proposed method needs to be improved for more complicated street environments. In future work, more features of point clusters, such as point density

and point distribution, can be used to distinguish street trees, and machine learning and deep learning algorithms can be introduced in our study to acquire more precise classification results.

### 5.2. Morphological Parameters Measurements

Morphological parameters of street trees measured in this study included tree height, crown width and diameter at breast height, which provide fundamental information about street trees.

The tree height measuring method utilizes the growing characteristic of trees and the results are of high precision. For crown width and DBH, point density is a vital factor that influenced the measuring methods for these two parameters. For street trees, points of tree crowns distribute unevenly, the part of tree crowns that closed to streets has higher point density, and point clouds of tree trunks are not integral. Considering the issue of uneven point density, results generated from circle-fitting and ellipse-fitting methods sometimes are not convincing. Crown width and DBH measuring methods proposed in this paper considers the characteristics of tree crown point clouds and tree trunk point clouds. The crown width measuring method could help avoid underestimating or overestimating crown widths. As for DBH, we adopt two measuring approaches. Street trees on Shuangxia Street and Taihu Street were of high point density, so trunk points at breast height were extracted to measure DBH. Street width of Bihua Street was wider than street widths of other two streets, so the point density of street trees on Bihua Street was lower, and measuring DBH of street trees required all trunk points of these trees. The precision of measuring results in our study were close to the precision of measuring results in Wu et al. [34], and the proposed measuring methods performed well when compared with other measuring methods [43]. However, DBH plays a crucial role in estimating the ecological benefits of trees, and the result of DBH measurements is not precise enough, thus improving the DBH measuring method is necessary in future work.

### 5.3. Carbon Sequestration and $PM_{2.5}$ Removal Estimation

Remote sensing methods, especially the combination of images (aerial or satellite) and LiDAR data, have been applied to estimate biomass, carbon storage, and map structures of urban forests in many studies [45–48]. However, most of these researches utilized ALS data and TLS data, and researches about utilizing MLS data or MLS-derived parameters to estimate carbon sequestration and pollutants removal are not common. In this study, tree heights and DBH of street trees generated from MLS data and tree species were imported to i-Tree Eco model to estimate carbon sequestration and  $PM_{2.5}$  removal of these trees.

When integral information are imported to i-Tree Eco model, carbon sequestration and leaf area can be obtained. According to the estimation results of each street tree, it is hard to conclude which trees species can bring greater ecological benefits for the urban environment. Carbon sequestration of trees is derived from tree biomass, and tree biomass is calculated based on allometric equations. The equations are distinct for different tree species. With respect to  $PM_{2.5}$  removal estimation, apart from leaf area, meteorological data and  $PM_{2.5}$  deposition velocities are also required, and deposition velocities vary considerably for different tree species. The decisive contributing factor that affects the estimation results of carbon sequestration and  $PM_{2.5}$  removal is tree species, which represents the natural properties of trees. For different tree species, tree height and DBH have limited influence on the estimation results of the two ecological benefits. While for the same tree species, the estimation results of carbon sequestration and  $PM_{2.5}$  would be mainly determined by tree height and DBH.

Tree height, DBH, and tree species are fundamental information for evaluating ecological benefits. To obtain more precise estimation results, the i-Tree Eco model requires more detailed information about trees, such as height to crown base and height to live top. In addition, there are no  $PM_{2.5}$  monitoring stations in study area, so  $PM_{2.5}$  concentrations data in the study area were replaced by the  $PM_{2.5}$  concentrations in Nantong City, which were not precise enough.  $PM_{2.5}$  deposition velocities of some tree species are not measured, and they have to be substituted by deposition velocities of

the same genus or deposition velocities of all broadleaf or conifer trees. The deficiency of PM<sub>2.5</sub> concentration data and deposition velocity data would create inaccuracies of the results.

Overall, estimation results of carbon sequestration and PM<sub>2.5</sub> presented in this paper is crude because of limited data and the equations used in the i-Tree Eco model [46]. However, the two ecological benefits generated from different tree species and different trees of the same species can be observed, and thus help to select tree species or trees that are more beneficial to urban street environments.

## 6. Conclusions

This work has proven that using raw MLS data to obtain morphological information and evaluate ecological benefits of individual urban street trees rapidly is feasible. The accuracy and efficiency of street trees extraction are improved by utilizing the method proposed in our study. Morphological parameters of each street tree, including tree height, crown width and DBH, are measured, enabling us to evaluate the ecological benefits of each street tree. Carbon sequestration and PM<sub>2.5</sub> removal of street trees can be obtained by importing the required information into the i-Tree Eco model. Our results suggest that ecological benefits are varied for different tree species, and for trees of the same species, ecological benefits are not the same. In order to obtain estimation results with higher accuracy, more sufficient and detailed data of street trees and the urban environment need to be collected. Additionally, understanding physiological characteristics of street trees can assist our understanding of the mechanism of ecological benefit generation, and physiological characteristics can be obtained with the help of spectral information. Therefore, in further study, spectral data of trees can be incorporated into research data to improve ecological benefits estimation results. Urban planners will be able to identify street trees that are more suitable for cities based on their ecological benefits.

**Author Contributions:** Conceptualization, Y.Z. and Q.H.; methodology, Y.Z. and Q.H.; software, Y.Z.; formal analysis, S.W.; investigation, H.L.; resources, S.W.; data curation, M.A.; writing—original draft preparation, Y.Z.; writing—review and editing, Q.H and H.L.; visualization, M.A.; supervision, Q.H.; project administration, Q.H.; funding acquisition, H.L.

**Funding:** This research received no external funding.

**Acknowledgments:** This research was supported by the National Key R&D Program of China, grant number No. 2017YFD0600904, and The Fundamental Research Funds for the Central Universities, grant number No. 2042017kf0235. This research was also supported by the Key Laboratory for National Geographic Census and Monitoring, National Administration of Surveying, Mapping and Geoinformation, grant number No. 2016NGCMZD01.

**Conflicts of Interest:** The authors declare no conflict of interest. The funders had no role in the design of the study; in the collection, analyses, or interpretation of data; in the writing of the manuscript, or in the decision to publish the results.

## References

1. Rantzoudi, E.C.; Georgi, J.N. Correlation between the geometrical characteristics of streets and morphological features of trees for the formation of tree lines in the urban design of the city of Orestiada, Greece. *Urban Ecosyst.* **2017**, *20*, 1081–1093. [[CrossRef](#)]
2. Nowak, D.J.; Crane, D.E. Carbon storage and sequestration by urban trees in the USA. *Environ. Pollut.* **2002**, *116*, 381–389. [[CrossRef](#)]
3. Jim, C.Y. A planning strategy to augment the diversity and biomass of roadside trees in urban Hong Kong. *Landsc. Urban Plan.* **1999**, *44*, 13–32. [[CrossRef](#)]
4. Coutts, A.M.; White, E.C.; Tapper, N.J.; Beringer, J.; Livesley, S.J. Temperature and human thermal comfort effects of street trees across three contrasting street canyon environments. *Theor. Appl. Climatol.* **2016**, *124*, 55–68. [[CrossRef](#)]
5. Alonzo, M.; Bookhagen, B.; Roberts, D.A. Urban tree species mapping using hyperspectral and lidar data fusion. *Remote Sens. Environ.* **2014**, *148*, 70–83. [[CrossRef](#)]
6. Li, X.; Zhang, C.; Li, W.; Ricard, R.; Meng, Q.; Zhang, W. Assessing street-level urban greenery using Google Street View and a modified green view index. *Urban For. Urban Green.* **2015**, *14*, 675–685. [[CrossRef](#)]

7. Pauleit, S. Urban street tree plantings: Identifying the key requirements. *Proc. Inst. Civ. Eng.-Munic. Eng.* **2003**, *156*, 43–50. [[CrossRef](#)]
8. Seiferling, I.; Naik, N.; Ratti, C.; Proulx, R. Green streets—Quantifying and mapping urban trees with street-level imagery and computer vision. *Landsc. Urban Plan.* **2017**, *165*, 93–101. [[CrossRef](#)]
9. Tallis, M.; Taylor, G.; Sinnett, D.; Freer-Smith, P. Estimating the removal of atmospheric particulate pollution by the urban tree canopy of London, under current and future environments. *Landsc. Urban Plan.* **2011**, *103*, 129–138. [[CrossRef](#)]
10. Chen, Z.; Xu, B.; Gao, B. Assessing visual green effects of individual urban trees using airborne Lidar data. *Sci. Total Environ.* **2015**, *536*, 232–244. [[CrossRef](#)] [[PubMed](#)]
11. Dobbs, C.; Escobedo, F.J.; Zipperer, W.C. A framework for developing urban forest ecosystem services and goods indicators. *Landsc. Urban Plan.* **2011**, *99*, 196–206. [[CrossRef](#)]
12. Chen, X.; Pei, T.; Zhou, Z.; Teng, M.; He, L.; Luo, M.; Liu, X. Efficiency differences of roadside greenbelts with three configurations in removing coarse particles (PM10): A street scale investigation in Wuhan, China. *Urban For. Urban Green.* **2015**, *14*, 354–360. [[CrossRef](#)]
13. Nowak, D.J.; Hirabayashi, S.; Bodine, A.; Hoehn, R. Modeled PM2.5 removal by trees in ten US cities and associated health effects. *Environ. Pollut.* **2013**, *178*, 395–402. [[CrossRef](#)] [[PubMed](#)]
14. Kiss, M.; Takács, Á.; Pogácsás, R.; Gulyás, Á. The role of ecosystem services in climate and air quality in urban areas: Evaluating carbon sequestration and air pollution removal by street and park trees in Szeged (Hungary). *Morav. Geogr. Rep.* **2015**, *23*, 36–46. [[CrossRef](#)]
15. Selmi, W.; Weber, C.; Rivière, E.; Blond, N.; Mehdi, L.; Nowak, D. Air pollution removal by trees in public green spaces in Strasbourg city, France. *Urban For. Urban Green.* **2016**, *17*, 192–201. [[CrossRef](#)]
16. Intasen, M.; Hauer, R.J.; Werner, L.P.; Larsen, E. Urban forest assessment in Bangkok, Thailand. *J. Sustain. For.* **2017**, *36*, 148–163. [[CrossRef](#)]
17. Nowak, D.J.; Greenfield, E.J.; Hoehn, R.E.; Lapoint, E. Carbon storage and sequestration by trees in urban and community areas of the United States. *Environ. Pollut.* **2013**, *178*, 229–236. [[CrossRef](#)] [[PubMed](#)]
18. Nowak, D.J.; Crane, D.E.; Stevens, J.C.; Hoehn, R.E.; Walton, J.T.; Bond, J. A ground-based method of assessing urban forest structure and ecosystem services. *Arboric. Urban For.* **2008**, *34*, 347–358.
19. Singh, K.K.; Chen, G.; McCarter, J.B.; Meentemeyer, R.K. Effects of LiDAR point density and landscape context on estimates of urban forest biomass. *ISPRS J. Photogramm. Remote Sens.* **2015**, *101*, 310–322. [[CrossRef](#)]
20. Bouvet, A.; Mermoz, S.; Le Toan, T.; Villard, L.; Mathieu, R.; Naidoo, L.; Asner, G.P. An above-ground biomass map of African savannahs and woodlands at 25m resolution derived from ALOS PALSAR. *Remote Sens. Environ.* **2018**, *206*, 156–173. [[CrossRef](#)]
21. Greaves, H.E.; Vierling, L.A.; Eitel, J.U.; Boelman, N.T.; Magney, T.S.; Prager, C.M.; Griffin, K.L. Estimating aboveground biomass and leaf area of low-stature Arctic shrubs with terrestrial LiDAR. *Remote Sens. Environ.* **2015**, *164*, 26–35. [[CrossRef](#)]
22. Holopainen, M.; Kankare, V.; Vastaranta, M.; Liang, X.; Lin, Y.; Vaaja, M.; Yu, X.; Hyyppä, J.; Hyyppä, H.; Kaartinen, H.; et al. Tree mapping using airborne, terrestrial and mobile laser scanning—A case study in a heterogeneous urban forest. *Urban For. Urban Green.* **2013**, *12*, 546–553. [[CrossRef](#)]
23. Estornell, J.; Ruiz, L.A.; Velázquez-Martí, B.; López-Cortés, I.; Salazar, D.; Fernández-Sarría, A. Estimation of pruning biomass of olive trees using airborne discrete-return LiDAR data. *Biomass Bioenergy* **2015**, *81*, 315–321. [[CrossRef](#)]
24. Lin, C.; Coops, N.C.; Hermosilla, T.; Innes, J.; Dai, J.S.; She, G.H. Using small-footprint discrete and full-waveform airborne lidar metrics to estimate total biomass and biomass components in subtropical forests. *Remote Sens.* **2014**, *6*, 7110–7135.
25. Cao, L.; Gao, S.; Li, P.; Yun, T.; Shen, X.; Ruan, H. Aboveground biomass estimation of individual trees in a coastal planted forest using full-waveform airborne laser scanning data. *Remote Sens.* **2016**, *8*, 729. [[CrossRef](#)]
26. Coomes, D.A.; Dalponte, M.; Jucker, T.; Asner, G.P.; Banin, L.F.; Burslem, D.F.; Lewis, S.L.; Nilus, R.; Phillips, O.L.; Phua, M.; et al. Area-based vs tree-centric approaches to mapping forest carbon in Southeast Asian forests from airborne laser scanning data. *Remote Sens. Environ.* **2017**, *194*, 77–88. [[CrossRef](#)]
27. Ene, L.T.; Næsset, E.; Gobakken, T.; Mauya, E.W.; Bollandssås, O.M.; Gregoire, T.G.; Ståhl, G.; Zahabu, E. Large-scale estimation of aboveground biomass in miombo woodlands using airborne laser scanning and national forest inventory data. *Remote Sens. Environ.* **2016**, *186*, 626–636. [[CrossRef](#)]

28. Matasci, G.; Hermosilla, T.; Wulder, M.A.; White, J.C.; Coops, N.C.; Hobart, G.W.; Zald, H.S. Large-area mapping of Canadian boreal forest cover, height, biomass and other structural attributes using Landsat composites and lidar plots. *Remote Sens. Environ.* **2018**, *209*, 90–106. [[CrossRef](#)]
29. Kankare, V.; Holopainen, M.; Vastaranta, M.; Puttonen, E.; Yu, X.; Hyypä, J.; Vaaja, M.; Hyypä, H.; Alho, P. Individual tree biomass estimation using terrestrial laser scanning. *ISPRS J. Photogramm. Remote Sens.* **2013**, *75*, 64–75. [[CrossRef](#)]
30. Lin, Y.; Jaakkola, A.; Hyypä, J.; Kaartinen, H. From TLS to VLS: Biomass estimation at individual tree level. *Remote Sens.* **2010**, *2*, 1864–1879. [[CrossRef](#)]
31. Xiao, W.; Vallet, B.; Brédif, M.; Paparoditis, N. Street environment change detection from mobile laser scanning point clouds. *ISPRS J. Photogramm. Remote Sens.* **2015**, *107*, 38–49. [[CrossRef](#)]
32. Zhang, C.; Zhou, Y.; Qiu, F. Individual tree segmentation from LiDAR point clouds for urban forest inventory. *Remote Sens.* **2015**, *7*, 7892–7913. [[CrossRef](#)]
33. Wang, J.; Lindenbergh, R.; Menenti, M. SigVox-A 3D feature matching algorithm for automatic street object recognition in mobile laser scanning point clouds. *ISPRS J. Photogramm. Remote Sens.* **2017**, *128*, 111–129. [[CrossRef](#)]
34. Wu, B.; Yu, B.; Yue, W.; Shu, S.; Tan, W.; Hu, C.; Huang, Y.; Wu, J.; Liu, H. A voxel-based method for automated identification and morphological parameters estimation of individual street trees from mobile laser scanning data. *Remote Sens.* **2013**, *5*, 584–611. [[CrossRef](#)]
35. Yang, B.; Dong, Z.; Zhao, G.; Dai, W. Hierarchical extraction of urban objects from mobile laser scanning data. *ISPRS J. Photogramm. Remote Sens.* **2015**, *99*, 45–57. [[CrossRef](#)]
36. Zhang, W.; Qi, J.; Wan, P.; Wang, H.; Xie, D.; Wang, X.; Yan, G. An easy-to-use airborne LiDAR data filtering method based on cloth simulation. *Remote Sens.* **2016**, *8*, 501. [[CrossRef](#)]
37. Maas, H.G.; Bienert, A.; Scheller, S.; Keane, E. Automatic forest inventory parameter determination from terrestrial laser scanner data. *Int. J. Remote Sens.* **2008**, *29*, 1579–1593. [[CrossRef](#)]
38. Yu, X.; Hyypä, J.; Vastaranta, M.; Holopainen, M.; Viitala, R. Predicting individual tree attributes from airborne laser point clouds based on the random forests technique. *ISPRS J. Photogramm. Remote Sens.* **2011**, *66*, 28–37. [[CrossRef](#)]
39. Fitzgibbon, A.; Pilu, M.; Fisher, R.B. Direct least square fitting of ellipses. *IEEE Trans. Pattern Anal. Mach. Intell.* **1999**, *21*, 476–480. [[CrossRef](#)]
40. Cao, H.; Yin, S.; Zhang, X.; Xiong, F.; Zhu, P.; Liu, C. Modeled PM2.5 removal by urban forest in Shanghai. *J. Shanghai Jiaotong Univ. Agric. Sci.* **2016**, *34*, 76–83.
41. Nowak, D.J. Estimating leaf area and leaf biomass of open-grown deciduous urban trees. *For. Sci.* **1996**, *42*, 504–507.
42. Li, L.; Li, D.; Zhu, H.; Li, Y. A dual growing method for the automatic extraction of individual trees from mobile laser scanning data. *ISPRS J. Photogramm. Remote Sens.* **2016**, *120*, 37–52. [[CrossRef](#)]
43. Tao, S.; Wu, F.; Guo, Q.; Wang, Y.; Li, W.; Xue, B.; Hu, X.; Li, P.; Tian, D.; Li, C.; et al. Segmenting tree crowns from terrestrial and mobile lidar data by exploring ecological theories. *ISPRS J. Photogramm. Remote Sens.* **2015**, *110*, 66–76. [[CrossRef](#)]
44. Lehtomäki, M.; Jaakkola, A.; Hyypä, J.; Lampinen, J.; Kaartinen, H.; Kukko, A.; Puttonen, E.; Hyypä, H. Object classification and recognition from mobile laser scanning point clouds in a road environment. *IEEE Trans. Geosci. Remote Sens.* **2016**, *54*, 1226–1239. [[CrossRef](#)]
45. Lee, J.H.; Ko, Y.; McPherson, E.G. The feasibility of remotely sensed data to estimate urban tree dimensions and biomass. *Urban For. Urban Green.* **2016**, *16*, 208–220. [[CrossRef](#)]
46. Alonzo, M.; McFadden, J.P.; Nowak, D.J.; Roberts, D.A. Mapping urban forest structure and function using hyperspectral imagery and lidar data. *Urban For. Urban Green.* **2016**, *17*, 135–147. [[CrossRef](#)]
47. Parmher, E.G.; Amati, M.; Taylor, E.J.; Livesley, S.J. Estimation of urban tree canopy cover using random point sampling and remote sensing methods. *Urban For. Urban Green.* **2016**, *20*, 160–171. [[CrossRef](#)]
48. Raciti, S.M.; Huttyra, L.R.; Newell, J.D. Mapping carbon storage in urban trees with multi-source remote sensing data: Relationships between biomass, land use, and demographics in Boston neighborhoods. *Sci. Total Environ.* **2014**, *500–501*, 72–83. [[CrossRef](#)] [[PubMed](#)]

